Applied Physics Letters

Electrical and optical characterizations of spin-orbit torque

Cite as: Appl. Phys. Lett. **118**, 072405 (2021); https://doi.org/10.1063/5.0045091
Submitted: 23 January 2021 . Accepted: 01 February 2021 . Published Online: 16 February 2021

Hanshen Huang, Hao Wu, Tian Yu, Quanjun Pan, Bingqian Dai, Armin Razavi, Kin Wong, Baoshan Cui, Su Kong Chong, Di Wu, and Kang L. Wang

AIP Publishing

Applied Physics Letters ARTICLE scitation.org/journal/apl

Electrical and optical characterizations of spin-orbit torque

Cite as: Appl. Phys. Lett. **118**, 072405 (2021); doi: 10.1063/5.0045091
Submitted: 23 January 2021 · Accepted: 1 February 2021 ·
Published Online: 16 February 2021

Hanshen Huang, Hao Wu,[a] Tian Yu, Quanjun Pan, Bingqian Dai, Armin Razavi, Kin Wong, Baoshan Cui, Su Kong Chong, Di Wu, and Kang L. Wang

AFFILIATIONS

Department of Electrical and Computer Engineering, Department of Physics and Astronomy, and Department of Material Science and Engineering, University of California, Los Angeles, California 90095, USA

Note: This paper is part of the Special Topic on Spin-Orbit Torque (SOT): Materials, Physics and Devices.
[a]**Author to whom correspondence should be addressed:** wuhaophysics@ucla.edu

ABSTRACT

To further reduce the energy consumption in spin–orbit torque devices, it is crucial to precisely quantify the spin–orbit torque (SOT) in different materials and structures. In this work, heavy metal/ferromagnet and heavy metal/ferrimagnet heterostructures are employed as the model systems to compare the electrical and optical methods for the SOT characterization, which are based on the anomalous Hall effect and the magneto-optical Kerr effect, respectively. It is found that both methods yield the consistent SOT strength for the current-driven magnetization switching measurements and the harmonic measurements. Our results suggest that the optical method is a feasible and reliable tool to investigate SOT, which is a powerful way to develop insulator-based magnetic systems in the future.

Spin–orbit torque (SOT) is a powerful way to manipulate magnetization electrically, which exhibits great potential in next-generation magnetic memory and logic applications. SOT-induced magnetization switching has been realized in abundant materials and structures, including heavy metal/ferromagnet heterostructures,[1–3] heavy metal/magnetic insulator heterostructures,[4–7] topological insulator/ferromagnet (ferrimagnet) heterostructures,[8–12] and magnetic topological insulators.[13–15] Also, much effort has been made to realize field-free SOT switching,[16–21] which paves the way for all-electrical SOT applications.

Conventionally, SOT is characterized electrically based on the anomalous Hall effect (AHE) or the tunneling magnetoresistance (TMR) effect.[22–24] However, the electrical method is limited by its complex signal origins and choice of materials. On the one hand, electrical signals originating from sources other than SOT, such as the current-induced thermal effects and the unidirectional magnetoresistance,[25,26] may obscure the characterization. On the other hand, for magnetic insulators (MIs), the electrical detection strongly relies on the interfacial proximity effect between the MIs and the conductors, resulting in an extremely small signal and instability in the SOT characterization.[27–29] Third, the optical method is a powerful way to detect the ultrafast SOT dynamics down to sub-picosecond.[30]

In this work, both electrical transport and optical methods are employed to characterize the SOT in ferromagnetic and ferrimagnetic heterostructures. To be more specific, films with stack of Ta(5)/CoFeB(1.1)/MgO(2)/Ta(2) and Ta(5)/GdFeCo(4)/MgO(2)/Ta(2) (unit in nm) are used as our model structures. Figures 1(a) and 1(b) show the lattice structure for CoFeB and GdFeCo, respectively. It is known that CoFeB is a typical ferromagnet, in which the spin of Co and Fe atoms points in the same direction, while for the ferrimagnetic GdFeCo, the spin sublattices of Gd and FeCo are antiferromagnetically coupled due to the atomic-level interfacial magnetic anisotropy, where the exchange magnetic resonance mode gives rise to the ultrafast ferrimagnetic spin dynamics beyond 100 GHz.[31–33] The films are grown by the magnetron sputtering with the base pressure lower than 5×10^{-8} Torr. The ferrimagnetic GdFeCo is deposited by co-sputtering Gd and CoFe targets, where its composition is controlled by tuning the sputtering power. To further enhance the perpendicular magnetic anisotropy (PMA) of Ta/CoFeB/MgO/Ta, post-annealing is carried out at 250 °C. These films are then patterned into 20 μm $\times$130 μm Hall-bar devices by standard photolithography combined with the dry etching method.

The electrical transport measurements are based on the AHE, where a Keithley 2612a source meter is used for generating the writing pulse current with a width of 1 ms, and the magnetization of the

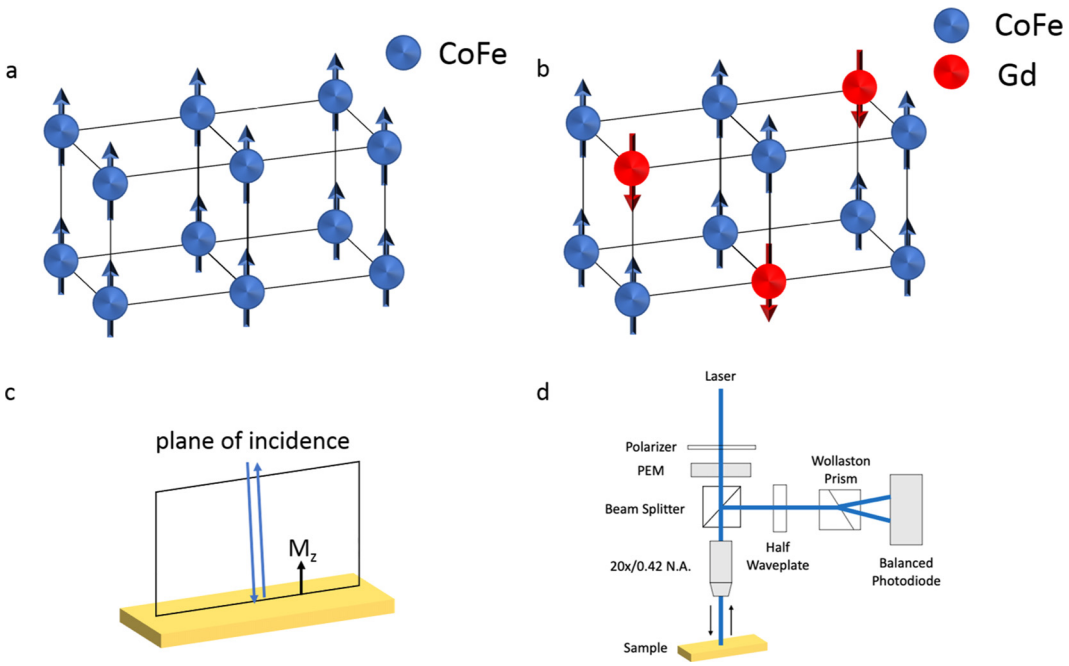

FIG. 1. Lattice structure of CoFeB (a) and GdFeCo (b); the blue balls stand for CoFe atoms, and red balls stand for Gd atoms. (c) Polar MOKE configuration. (d) Schematic of the polar MOKE setup for the optical measurement.

devices is subsequently read by applying a small reading current of 0.1 mA to minimize the thermal effects. The optical measurements are conducted based on the magneto-optic Kerr effect (MOKE) in the polar configuration,[34] as shown in Fig. 1(c), where the rotated polarization angle of the reflected light is proportional to the out-of-plane component of magnetization (M_z). The optical measurement setup is shown in Fig. 1(d). A laser light source of 410 nm is deployed for optical measurements. To further improve the signal-to-noise ratio, a photoelastic modulator (PEM) is adopted and its modulation rate is kept at 100 kHz. The incident light is linearly polarized and focused onto the devices using a microscope (20×/0.42 NA, spot size ∼10 μm). The reflected light is separated into *s* polarized light and *p* polarized light by a Wollaston prism and then collected by a balanced photodiode. The Kerr rotation angle and, thus, magnetization of the devices are demodulated and detected using a lock-in amplifier. All measurements are conducted at room temperature.

Magnetic materials with PMA are preferred for high-density and low-energy consumption memory applications.[35] We first evaluate the PMA for Ta/CoFeB/MgO/Ta and Ta/GdFeCo/MgO/Ta by measuring their in-plane saturation field (hard axis),[36] from which the anisotropy fields (H_k) are estimated to be 1470 Oe and 2731 Oe, respectively. The PMA is also identified by measuring anomalous Hall resistance (R_{xy}) as a function of magnetic field along the out-of-plane direction (H_z), as shown in Figs. 2(a) and 2(b), where the sharp switching in the R_{xy}-H_z loops clearly indicates the strong PMA. Similar results are obtained in the polar MOKE measurements, where the magnetization information is represented by the Kerr rotation angle (θ_K) instead of R_{xy}. As seen in Figs. 2(c) and 2(d), the θ_K-H_z loops resemble the results in the electrical transport method. Unlike the electrical transport measurement that averages the magnetization across the whole device, the optical method detects local magnetization beneath the laser spot, and we attribute the slight coercivity difference between the electrical transport and optical measurements for GdFeCo to the magnetic inhomogeneity across the device.

By applying a fixed in-plane magnetic field ($H_x = 55$ Oe) to break the symmetry between up and down magnetizations, the current-induced SOT could switch the perpendicular magnetization deterministically.[18] This deterministic SOT switching is characterized by both electrical transport and optical methods. As indicated by the changes in R_{xy} in Figs. 3(a) and 3(d), the magnetization is switched by sweeping the writing current. The critical switching current densities for Ta/CoFeB/MgO/Ta and Ta/GdFeCo/MgO/Ta estimated from R_{xy}-J_e loops are 8.2×10^6 A cm^{-2} and 1.1×10^7 A cm^{-2}, respectively. It is also shown in Figs. 3(a) and 3(d) that the polarity of the SOT-induced magnetization switching reverses correspondingly as we reverse the in-plane bias field, which confirms the SOT characteristic. In the optical measurements, the readout of the SOT switching is accomplished by recording the θ_K-J_e loops. As shown in Figs. 3(b) and 3(e), the θ_K vs J_e curve is similar to the R_{xy} vs J_e curve by the electrical method, suggesting that θ_K is equivalent to R_{xy} in characterizing the SOT switching.

Nevertheless, the optical method further provides us the ability to visualize the magnetic domain changes during the SOT switching. This is demonstrated in Figs. 3(c) and 3(f) by implementing the same principle as the above polar MOKE measurements but using a charge-coupled device (CCD) to obtain a spatial resolution of magnetic domains. The contrast of the MOKE image represents the magnetic domain state, i.e., the bright and dark contrast corresponds to the up

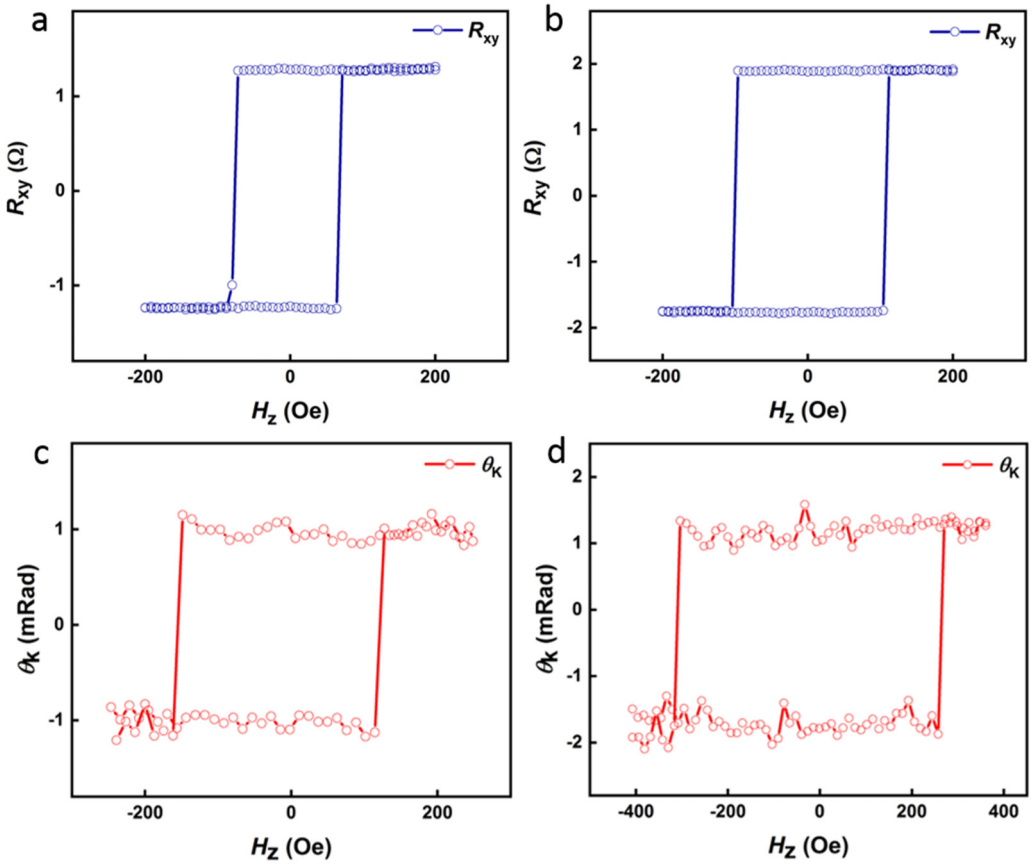

FIG. 2. Hysteresis loops of (a) Ta/CoFeB/MgO/Ta by the transport measurement. (b) Ta/GdFeCo/MgO/Ta by the transport measurement. (c) Ta/CoFeB/MgO/Ta by the optical measurement. (d) Ta/GdFeCo/MgO/Ta by the optical measurement.

and down magnetic domains, respectively. The MOKE images not only characterize the initial and final states of the magnetic domains in the devices but also visualize the whole switching process. For example, in CoFeB heterostructures [Fig. 3(c)], the magnetic domain nucleates at the right end of the Hall bar device first. As we increased the writing current density gradually, the domain wall propagates from the right side to the left side to realize the full magnetization switching.

The SOT strength is further investigated by the electrical transport method and the optical MOKE method, respectively. In the electrical transport measurements, conventional first and second harmonic signals are measured by sweeping the magnetic field in the film plane. A sinusoidal modulation current at a frequency of 273 Hz is mixed with the writing current ($J_e = 2.46 \times 10^6$ A cm^{-2} and $J_e = 1.67 \times 10^6$ A cm^{-2} for the CoFeB and GdCoFe stacks, respectively). During the electrical transport measurements, the laser continuously illuminates the samples to ensure the same thermal condition as that in the optical measurements. Figures 4(a)–4(d) show the harmonic signals measured by the electrical transport method for Ta/CoFeB/MgO/Ta and Ta/GdCoFe/MgO/Ta, respectively. When the applied field H_x is larger than the anisotropy field H_k, the magnetization is aligned along the in-plane direction and the out-of-plane oscillation is mainly due to the sinusoidal current modulation-induced damping-like torque. Thus, the tilting angle can be expressed as[37–39]

$$\Delta\theta_M = -\frac{H_{DL}}{|H_x| - H_k}\sin\omega t, \tag{1}$$

where ω is the current frequency, H_{DL} is the damping-like effective field, and H_k is the anisotropy field. As the planar Hall effect is negligible in these two heterostructures, the Hall resistance can be written as

$$R_{xy} = R_{AHE}\cos(\theta + \Delta\theta_M)\sin\omega t, \tag{2}$$

where R_{AHE} is the anomalous Hall resistance and θ is the angle between magnetization and the z-axis direction $\left(\theta = \frac{\pi}{2}\right)$. Expanding Eq. (2) and taking the thermal contribution R_{SSE} into account, we can obtain the second harmonic Hall resistance as follows:

$$R_{xy}^{2\omega} = -\frac{R_{AHE}}{2}\frac{H_{DL}}{|H_x| - H_k} + R_{SSE}\frac{H_x}{|H_x|} + R_{offset}, \tag{3}$$

where R_{offset} is the offset background. By fitting the experimental data with Eq. (3), it is found that the damping-like effective fields (H_{DL}) are 3.09 Oe and 2.54 Oe for the CoFeB and GdFeCo heterostructures, respectively, which implies that the SOT coefficient ($\chi_{SOT} = H_{DL}/J_e$) and the effective spin Hall angle ($|\theta_{SH}| = (2|e|M_s t_F/\hbar)\chi_{SOT}$) are 1.26×10^{-6} Oe A^{-1} cm^2 and 0.04 for the Ta/CoFeB stack, and 1.52×10^{-6} Oe A^{-1} cm^2 and 0.03 for the Ta/GdFeCo stack, respectively.

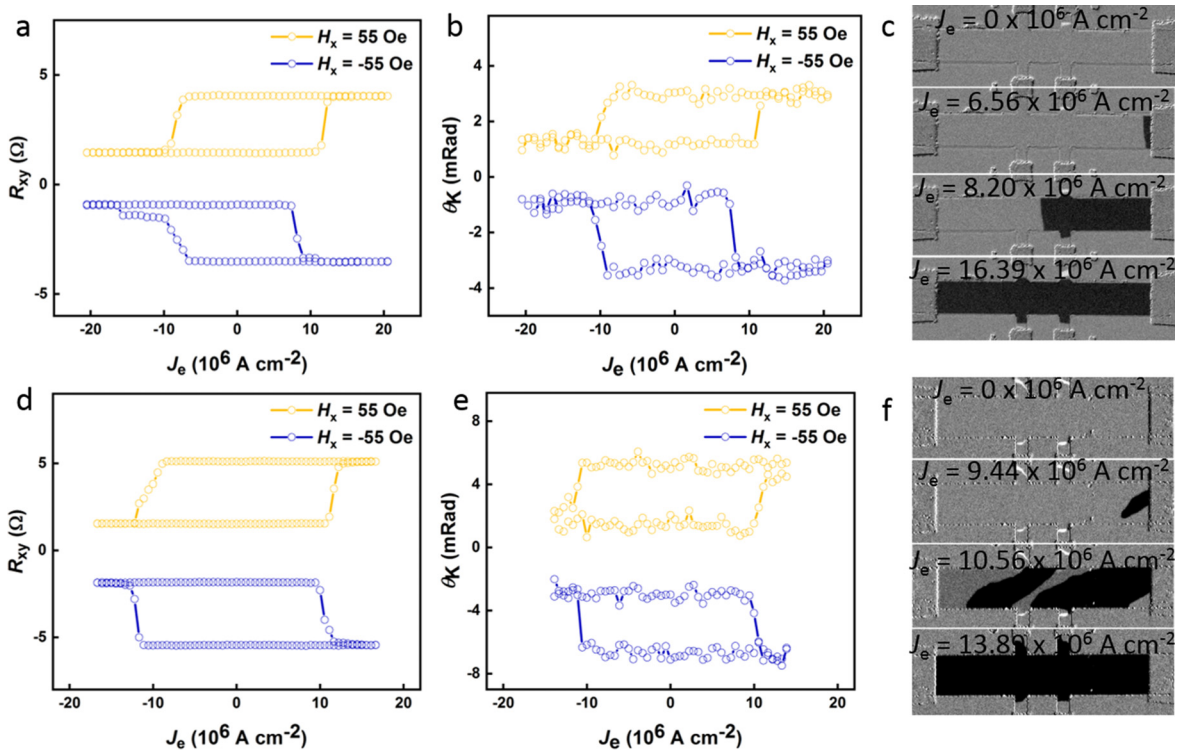

FIG. 3. SOT-induced magnetization switching measured by transport and optical methods for Ta/CoFeB/MgO/Ta (a)–(c) and Ta/GdFeCo/MgO/Ta (d)–(f). The magnetic domain states at different current densities indicate the domain nucleation and domain wall propagation switching mechanism.

A similar setup as shown in Fig. 1(d) is used for determining these parameters optically. The first harmonic measurement is the same as that conducted in electrical transport measurements except now θ_K is recoded and the lock-in frequency is chosen as the PEM modulation frequency. The optical counterpart of the second harmonic measurement is also known as the differential Kerr method ($\Delta\theta_K$). Following the derivation in the supplementary material of reference,[4] the Kerr rotation θ_K can be expanded using the Taylor expansion as

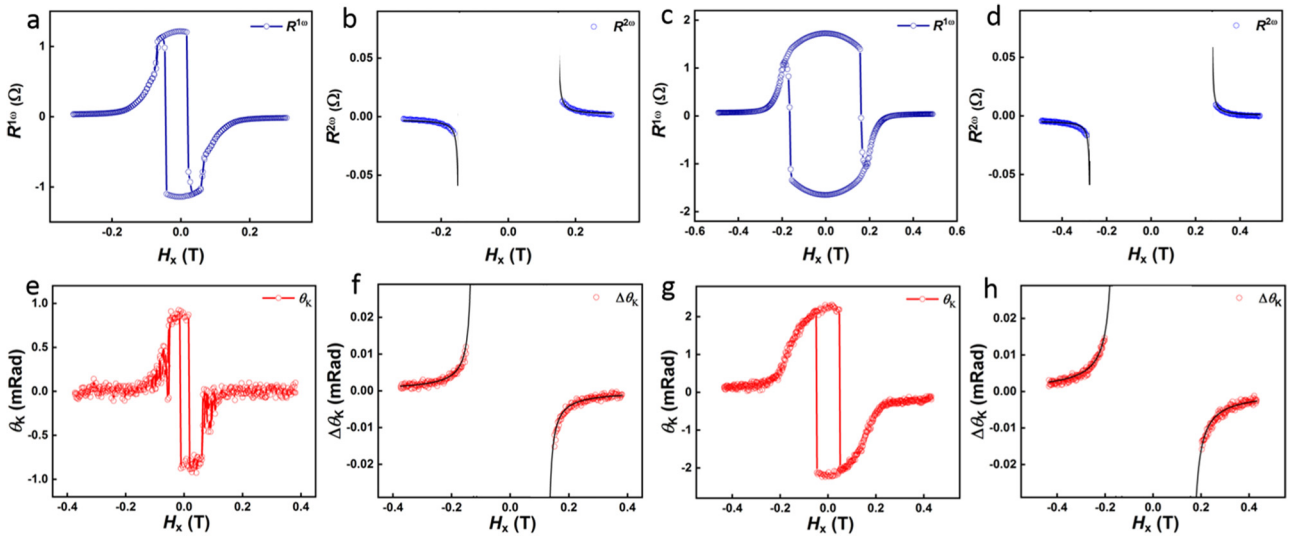

FIG. 4. First harmonic (a) and (c) and second harmonic Hall resistance (b) and (d) by the transport method for Ta/CoFeB/MgO/Ta (a) and (b) and Ta/GdFeCo/MgO/Ta (c) and (d). Kerr rotation (e) and (g) and differential Kerr rotation (f) and (h) by the optical method for Ta/CoFeB/MgO/Ta (e) and (g) and Ta/GdFeCo/MgO/Ta (f) and (h).

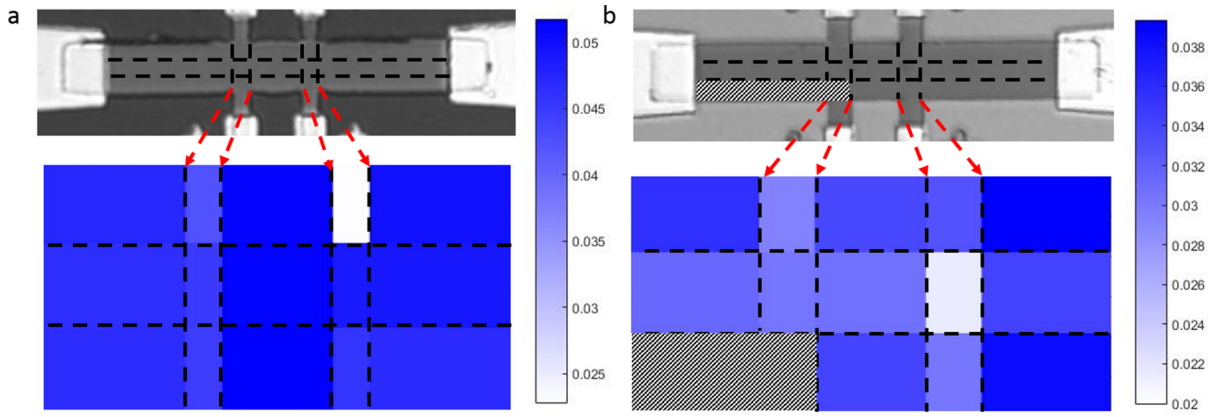

FIG. 5. Spatial mapping of the effective spin Hall angle on (a) Ta/CoFeB/MgO/Ta and (b) Ta/GdFeCo/MgO/Ta heterostructure Hall bar devices (the lower left corner is not measured).

$$\theta_K = \theta_{K0} + \Delta\theta_K \sin \omega t, \tag{4}$$

where θ_{K0} is the Kerr rotation angle without applying current and ω is the current frequency. By setting the zero net torque condition, we have $\boldsymbol{m} \times \boldsymbol{H} = 0$, where $\boldsymbol{m}$ and $\boldsymbol{H}$ are the magnetization and magnetic field, respectively. Since the second order magneto-optic effect is much smaller than that of the first order, we only consider the first-order term here. Thus, we are able to obtain the expression similar to $R_{xy}^{2\omega}$ in the electrical transport measurement for $\Delta\theta_K$,

$$\Delta\theta_K = \frac{f H_{DL}}{|H_x| - H_k}, \tag{5}$$

where f is the magneto-optic coefficient. Based on the results of the optical method, as shown in Figs. 4(e)–4(h), the damping-like effective fields are 3.60 Oe and 3.32 Oe for Ta/CoFeB/MgO/Ta and Ta/GdFeCo/MgO/Ta, respectively, which are similar to those found by the electrical transport method and, thus, yield a similar SOT coefficient χ_{SOT} (1.47×10^{-6} Oe A^{-1} cm^2 for the Ta/CoFeB stack and 1.99×10^{-6} Oe A^{-1} cm^2 for the Ta/GdFeCo stack) and the effective spin Hall angle $|\theta_{SH}|$ (0.05 for the CoFeB stack and 0.04 for the GdFeCo stack).

To explore more advantages of the optical method, we further investigate the spatial distribution of SOT by the differential Kerr method. We divide the Hall bar device into fifteen representative areas as shown in Figs. 5(a) and 5(b) and used the differential Kerr method to extract the effective spin Hall angle in each area. Consequently, we obtain the spatial mapping of the effective spin Hall angle, which shows how the effective spin Hall angle fluctuates across the device. From the results, we can see that there is not much fluctuation in the CoFeB heterostructure. However, in the GdFeCo heterostructure, the effective spin Hall angles in the central regions (the second row) of the sample are 10% smaller than the edge areas (the first and the third row). One possible reason is that the CoFeB stack is less sensitive to temperature, which is not the case for the GdFeCo stack. When the sinusoidal current is injected into the current channel for the differential Kerr measurement, there will be a temperature distribution across the cross section of the device, which means that the temperature is higher in the middle of the device. According to reference,[40] for the FeCo-rich GdFeCo stack, saturation magnetization M_s is much larger with the increasing temperature. Therefore, the obtained SOT effective field and the calculated effective spin Hall angle are smaller. Besides, the effective spin Hall angle in the arm area of the Hall bar device (the first and the fifth column) is a bit larger than those in the cross area (the second and the fourth column), which can be attributed to the higher current density in the arm area due to the shunting effect.[41] In addition, we perform all optical methods on the unpatterned CoFeB stack and GdFeCo stack films as well (supplementary material). We can clearly observe the switching processes by MOKE imaging and optically extract the effective spin Hall angle by the differential Kerr method. This shows the feasibility of using all the optical method on unpatterned films, which can simplify the measurement by reducing the need for device fabrication.

In summary, we measure a series of magnetic and SOT properties, including the hysteresis loops, current-driven SOT switching, and first and second harmonic SOT signals, in Ta/CoFeB/MgO/Ta and Ta/GdFeCo/MgO/Ta heterostructures by both the electrical transport and the optical MOKE methods. Current-driven deterministic SOT switching is demonstrated by both the electrical transport Hall measurements and optical MOKE measurements. The magnetic domain switching process during the SOT switching is also visualized by the MOKE imaging technique, which suggests that the SOT switching is dominated by the magnetic domain nucleation and domain wall propagation process. The SOT strength is further quantified by the harmonic measurements based on both the electrical and the optical signals. It is demonstrated that the optical method gives consistent SOT parameters as those obtained in the conventional electrical transport measurements, which would be a powerful tool for investigating the SOT in insulating magnets in the future.

See the supplementary material for MOKE imaging of the switching process, Kerr rotation, and differential Kerr rotation measured on unpatterned films.

This work was supported by the NSF under Award Nos. 1935362, 1909416, 1810163, and 1611570, the Nanosystems

Engineering Research Center for Translational Applications of Nanoscale Multiferroic Systems (TANMS), the U.S. Army Research Office MURI program under Grant Nos. W911NF-16-1-0472 and WN911NF-20-2-0166, and the Spins and Heat in Nanoscale Electronic Systems (SHINES) Center funded by the U.S. Department of Energy (DOE), under Award No. DE-SC0012670.

DATA AVAILABILITY

The data that support the findings of this study are available from the corresponding author upon reasonable request.

REFERENCES

[1]L. Liu, C. F. Pai, Y. Li, H. W. Tseng, D. C. Ralph, and R. A. Buhrman, Science **336**(6081), 555–558 (2012).
[2]C. F. Pai, L. Liu, Y. Li, H. W. Tseng, D. C. Ralph, and R. A. Buhrman, Appl. Phys. Lett. **101**, 122404 (2012).
[3]I. M. Miron, K. Garello, G. Gaudin, P. J. Zermatten, M. V. Costache, S. Auffret, S. Bandiera, B. Rodmacq, A. Schuhl, and P. Gambardella, Nature **476**, 189–193 (2011).
[4]M. Montazeri, P. Upadhyaya, M. C. Onbasli, G. Yu, K. L. Wong, M. Lang, Y. Fan, X. Li, P. K. Amiri, R. N. Schwartz, C. A. Ross, and K. L. Wang, Nat. Commun. **6**, 8958 (2015).
[5]Q. Shao, C. Tang, G. Yu, A. Navabi, H. Wu, C. He, J. Li, P. Upadhyaya, P. Zhang, S. A. Razavi, Q. L. He, Y. Liu, P. Yang, S. K. Kim, C. Zheng, Y. Liu, L. Pan, R. K. Lake, X. Han, Y. Tserkovnyak, J. Shi, and K. L. Wang, Nat. Commun. **9**, 3612 (2018).
[6]C. O. Avci, A. Quindeau, C. F. Pai, M. Mann, L. Caretta, A. S. Tang, M. C. Onbasli, C. A. Ross, and G. S. D. Beach, Nat. Mater. **16**, 309–314 (2017).
[7]C. Y. Guo, C. H. Wan, M. K. Zhao, H. Wu, C. Fang, Z. R. Yan, J. F. Feng, H. F. Liu, and X. F. Han, Appl. Phys. Lett. **114**, 192409 (2019).
[8]J. Han, A. Richardella, S. A. Siddiqui, J. Finley, N. Samarth, and L. Liu, Phys. Rev. Lett. **119**, 077702 (2017).
[9]M. Dc, R. Grassi, J. Y. Chen, M. Jamali, D. Reifsnyder Hickey, D. Zhang, Z. Zhao, H. Li, P. Quarterman, Y. Lv, M. Li, A. Manchon, K. A. Mkhoyan, T. Low, and J. P. Wang, Nat. Mater. **17**, 800–807 (2018).
[10]N. H. D. Khang, Y. Ueda, and P. N. Hai, Nat. Mater. **17**, 808–813 (2018).
[11]Y. Wang, D. Zhu, Y. Wu, Y. Yang, J. Yu, R. Ramaswamy, R. Mishra, S. Shi, M. Elyasi, K. L. Teo, Y. Wu, and H. Yang, Nat. Commun. **8**, 1364 (2017).
[12]H. Wu, P. Zhang, P. Deng, Q. Lan, Q. Pan, S. A. Razavi, X. Che, L. Huang, B. Dai, K. Wong, X. Han, and K. L. Wang, Phys. Rev. Lett. **123**, 207205 (2019).
[13]Y. Fan, P. Upadhyaya, X. Kou, M. Lang, S. Takei, Z. Wang, J. Tang, L. He, L. Te Chang, M. Montazeri, G. Yu, W. Jiang, T. Nie, R. N. Schwartz, Y. Tserkovnyak, and K. L. Wang, Nat. Mater. **13**, 699–704 (2014).
[14]Y. Fan, X. Kou, P. Upadhyaya, Q. Shao, L. Pan, M. Lang, X. Che, J. Tang, M. Montazeri, K. Murata, L. Te Chang, M. Akyol, G. Yu, T. Nie, K. L. Wong, J. Liu, Y. Wang, Y. Tserkovnyak, and K. L. Wang, Nat. Nanotechnol. **11**, 352–359 (2016).
[15]K. Yasuda, A. Tsukazaki, R. Yoshimi, K. Kondou, K. S. Takahashi, Y. Otani, M. Kawasaki, and Y. Tokura, Phys. Rev. Lett. **119**, 137204 (2017).
[16]Y. C. Lau, D. Betto, K. Rode, J. M. D. Coey, and P. Stamenov, Nat. Nanotechnol. **11**, 758–762 (2016).
[17]Y. W. Oh, S. H. C. Baek, Y. M. Kim, H. Y. Lee, K. D. Lee, C. G. Yang, E. S. Park, K. S. Lee, K. W. Kim, G. Go, J. R. Jeong, B. C. Min, H. W. Lee, K. J. Lee, and B. G. Park, Nat. Nanotechnol. **11**, 878–884 (2016).
[18]G. Yu, P. Upadhyaya, Y. Fan, J. G. Alzate, W. Jiang, K. L. Wong, S. Takei, S. A. Bender, L. Te Chang, Y. Jiang, M. Lang, J. Tang, Y. Wang, Y. Tserkovnyak, P. K. Amiri, and K. L. Wang, Nat. Nanotechnol. **9**, 548–554 (2014).
[19]S. Fukami, C. Zhang, S. Duttagupta, A. Kurenkov, and H. Ohno, Nat. Mater. **15**, 535–541 (2016).
[20]S. H. C. Baek, V. P. Amin, Y. W. Oh, G. Go, S. J. Lee, G. H. Lee, K. J. Kim, M. D. Stiles, B. G. Park, and K. J. Lee, Nat. Mater. **17**, 509–513 (2018).
[21]A. Razavi, H. Wu, Q. Shao, C. Fang, B. Dai, K. Wong, X. Han, G. Yu, and K. L. Wang, Nano Lett. **20**, 3703–3709 (2020).
[22]T. Miyazaki and N. Tezuka, J. Magn. Magn. Mater. **139**(1995), L231–L297 (1995).
[23]M. Julliere, Phys. Lett. A **54**, 225–226 (1975).
[24]J. S. Moodera, L. R. Kinder, T. M. Wong, and R. Meservey, Phys. Rev. Lett. **74**, 3273–3276 (1995).
[25]C. O. Avci, K. Garello, A. Ghosh, M. Gabureac, S. F. Alvarado, and P. Gambardella, Nat. Phys. **11**, 570–575 (2015).
[26]K. Yasuda, A. Tsukazaki, R. Yoshimi, K. S. Takahashi, M. Kawasaki, and Y. Tokura, Phys. Rev. Lett. **117**, 127202 (2016).
[27]P. Li, J. Kally, S. S. L. Zhang, T. Pillsbury, J. Ding, G. Csaba, J. Ding, J. S. Jiang, Y. Liu, R. Sinclair, C. Bi, A. DeMann, G. Rimal, W. Zhang, S. B. Field, J. Tang, W. Wang, O. G. Heinonen, V. Novosad, A. Hoffmann, N. Samarth, and M. Wu, Sci. Adv. **5**(8), eaaw3415 (2019).
[28]S. Y. Huang, X. Fan, D. Qu, Y. P. Chen, W. G. Wang, J. Wu, T. Y. Chen, J. Q. Xiao, and C. L. Chien, Phys. Rev. Lett. **109**, 107204 (2012).
[29]H. Nakayama, M. Althammer, Y. T. Chen, K. Uchida, Y. Kajiwara, D. Kikuchi, T. Ohtani, S. Geprägs, M. Opel, S. Takahashi, R. Gross, G. E. W. Bauer, S. T. B. Goennenwein, and E. Saitoh, Phys. Rev. Lett. **110**, 206601 (2013).
[30]H. Wu, D. Turan, Q. Pan, G. Wu, S. A. Razavi, N. T. Yardimci, Z. Zhang, M. Jarrahi, and K. L. Wang, preprint arXiv:1912.10129 (2019).
[31]C. D. Stanciu, A. V. Kimel, F. Hansteen, A. Tsukamoto, A. Itoh, A. Kirilyuk, and T. Rasing, Phys. Rev. B **73**, 220402 (2006).
[32]I. Radu, K. Vahaplar, C. Stamm, T. Kachel, N. Pontius, H. A. Dürr, T. A. Ostler, J. Barker, R. F. L. Evans, R. W. Chantrell, A. Tsukamoto, A. Itoh, A. Kirilyuk, T. Rasing, and A. V. Kimel, Nature **472**, 205–208 (2011).
[33]H. Wu, F. Groß, B. Dai, D. Lujan, S. A. Razavi, P. Zhang, Y. Liu, K. Sobotkiewich, J. Förster, M. Weigand, G. Schütz, X. Li, J. Gräfe, and K. L. Wang, Adv. Mater. **32**(34), 2003380 (2020).
[34]S. Visnovsky and B. Thompson, *Optics in Magnetic Multilayers and Nanostructures* (CRC Press, Boca Raton, 2006).
[35]S. Mangin, D. Ravelosona, J. A. Katine, M. J. Carey, B. D. Terris, and E. E. Fullerton, Nat. Mater. **5**, 210–215 (2006).
[36]D. Wu, Z. Zhang, L. Li, Z. Zhang, H. B. Zhao, J. Wang, B. Ma, and Q. Y. Jin, Sci. Rep. **5**, 12352 (2015).
[37]H. Wu, Y. Xu, P. Deng, Q. Pan, S. A. Razavi, K. Wong, L. Huang, B. Dai, Q. Shao, G. Yu, X. Han, J. C. Rojas-Sánchez, S. Mangin, and K. L. Wang, Adv. Mater. **31**(35), 1901681 (2019).
[38]M. Hayashi, J. Kim, M. Yamanouchi, and H. Ohno, Phys. Rev. B **89**, 144425 (2014).
[39]Q. Shao, G. Yu, Y. W. Lan, Y. Shi, M. Y. Li, C. Zheng, X. Zhu, L. J. Li, P. K. Amiri, and K. L. Wang, Nano Lett. **16**(12), 7514–7520 (2016).
[40]Y. Hirata, D. Kim, T. Okuno, T. Nishimura, D. Kim, Y. Futakawa, H. Yoshikawa, A. Tsukamoto, K. Kim, S. Choe, and T. Ono, Phys. Rev. B **97**, 220403(R) (2018).
[41]T. Y. Tsai, T. Y. Chen, C. T. Wu, H. I. Chan, and C. F. Pai, Sci. Rep. **8**, 5613 (2018).